

The evolution of cold neutral gas and the star formation history

S. J. Curran*

School of Chemical and Physical Sciences, Victoria University of Wellington, PO Box 600, Wellington 6140, New Zealand

Accepted —. Received —; in original form —

ABSTRACT

There is a well known disparity between the evolution the star formation rate density, ψ_* , and the abundance of neutral hydrogen (H I), the raw material for star formation. Recently, however, we have shown that ψ_* may be correlated with the fraction of *cool* atomic gas, as traced through the 21-cm absorption of H I. This is expected since star formation requires cold ($T \sim 10$ K) gas and so this could address the issue of why the star formation rate density does not trace the bulk atomic gas. The data are, however, limited to redshifts of $z \lesssim 2$, where both ψ_* and the cold gas fraction exhibit a similar steep climb from the present day ($z = 0$), and so it is unknown whether the cold gas fraction follows the same decline as ψ_* at higher redshift. In order to address this, we have used unpublished archival observations of 21-cm absorption in high redshift damped Lyman- α absorption systems to increase the sample at $z \gtrsim 2$. The data suggest that the cold gas fraction does exhibit a decrease, although this is significantly steeper than ψ_* at $z \sim 3$. This is, however, degenerate with the extents of the absorbing galaxy and the background continuum emission and upon removing these, via canonical evolution models, we find the mean spin temperature of the gas to be $\langle T_{\text{spin}} \rangle \approx 3000$ K, compared to the ≈ 2000 K expected from the $\psi_* T_{\text{spin}} \approx 100 \text{ M}_\odot \text{ yr}^{-1} \text{ Mpc}^{-3} \text{ K}$ fit at $z \lesssim 2$. These temperatures are consistent with the observed high neutral hydrogen column densities, which require $T \lesssim 4000$ K in order for the gas not to be highly ionised.

Key words: galaxies: high redshift – galaxies: star formation – galaxies: evolution – galaxies: ISM – quasars: absorption lines – radio lines: galaxies

1 INTRODUCTION

Galaxies intervening the sight-lines to more distant Quasi-Stellar Objects (QSOs) allow study of the neutral gas in the distant Universe, through the absorption of the background continuum radiation by the Lyman- α ($\lambda = 1215.67 \text{ \AA}$) transition of hydrogen. These so-called *damped Lyman- α absorbers* (DLAs), where the neutral hydrogen column density exceeds $N_{\text{HI}} \geq 2 \times 10^{20} \text{ atoms cm}^{-2}$, may contain up to 80% of the neutral gas mass density in the Universe (Prochaska et al. 2005). The detection of this transition is restricted to redshifts of $z \gtrsim 1.7$ (the first four billion years of the Universe’s history) by ground-based telescopes, where this ultra-violet band transition is redshifted into the atmospheric window at visible wavelengths. Apart from space-based observations (e.g. Rao et al. 2017), hydrogen at lower redshifts can be detected through the spin-flip ($\lambda = 21.1 \text{ cm}$) transition, which occurs in the radio band.

Observations of both H I 21-cm emission (Zwaan et al. 2005b; Lah et al. 2007; Braun 2012; Delhaize et al. 2013; Rhee et al. 2013; Hoppmann et al. 2015) and Lyman- α absorption (Hopkins & Beacom 2006; Burgarella et al. 2013; Behroozi et al. 2013; Sobral et al. 2013; Madau & Dickinson 2014; Zwart et al.

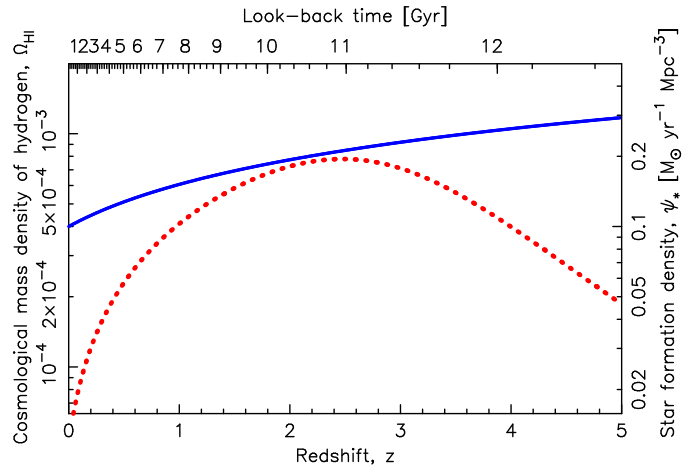


Figure 1. The cosmological mass density of neutral hydrogen (solid trace & left scale, Crighton et al. 2017) and the star formation density (dotted trace & right scale, Hopkins & Beacom 2006).

2014) show that there is little evolution in the mass density of neutral hydrogen, which is in stark contrast to the steep evolution in the cosmic star formation rate (Fig. 1). However, both

* Stephen.Curran@vuw.ac.nz

Lyman- α absorption and 21-cm emission trace all of the neutral gas ($T \lesssim 10\,000$ K), whereas only the gas clouds which are cool enough ($T \sim 10$ K) to collapse under their own gravity can initiate star formation. This cool component of the gas is detected through the *absorption* of the 21-cm radiation from a background radio-loud QSO (quasar). If the Lyman- α and 21-cm absorption trace the same sight-line, comparison of the 21-cm absorption strength with the total neutral hydrogen column density can, in principle, yield the spin temperature of the gas, T_{spin} , although this is degenerate with the fraction of the background radio flux intercepted by the absorbing gas.

Although this *covering factor* is difficult to quantify, by accounting for the angular diameter distances to the absorbing galaxy and background continuum source, we can at least remove any bias introduced by an expanding Universe from the flux coverage. This yields the spin temperature degenerate with the ratio of the projected sizes of the absorber and the continuum source, $T_{\text{spin}}(d_{\text{QSO}}/d_{\text{abs}})^2$. Using this method, we (Curran 2017a,b) have shown that the reciprocal of this, $(1/T_{\text{spin}})(d_{\text{abs}}/d_{\text{QSO}})^2$, increases by a similar amount as the star formation rate from $z_{\text{abs}} = 0$ to the peak of star formation at $z_{\text{abs}} \sim 2$. That is, for a non-evolving $d_{\text{abs}}/d_{\text{QSO}}$ ratio, the spin temperature is anti-correlated with ψ_* , as would be expected upon the basis that stars can only form out of the coldest gas. Being limited to $z_{\text{abs}} \lesssim 2$, however, means that we do not know whether $(1/T_{\text{spin}})(d_{\text{abs}}/d_{\text{QSO}})^2$ exhibits a downturn at higher redshift, thus truly tracing the star formation history, rather than a coincidental similar factor of increase over $0 \lesssim z_{\text{abs}} \lesssim 2$. In order to address this, here we add a dozen previously unpublished high redshift searches for 21-cm absorption in DLAs from the data archive of the Giant Metrewave Radio Telescope (GMRT).

2 DATA ACQUISITION AND REDUCTION

The GMRT is the longest serving large interferometer capable of observing at the required frequencies ($\lesssim 470$ MHz for 21-cm at $z \gtrsim 2$), thus having the most comprehensive archive, in addition to being able to reach the required sensitivities (Curran 2018). Radio frequency interference (RFI) meant that many of the sources in the archive could not be reduced and some flagging of badly affected data were required on the dozen remaining sight-lines (Table 1). These had all been observed using the full 30 antenna array, with 3C 48, 3C 147 and 3C 298 used for bandpass calibration and a nearby bright, unresolved radio source for phase calibration. Upon downloading the data, these were calibrated and flagged with the MIRIAD interferometry reduction package. For each of these sources, after calibration, the two polarisations were averaged and a cube produced, from which a spectrum was extracted (Fig. 2). The addition of these absorbers, takes the total number to 85, cf. the 74 previously (Curran 2017a).¹ All of the new absorbers have redshifts of $z_{\text{abs}} \geq 1.913$, where there are currently 36 DLAs with published searches for 21-cm absorption.²

¹ From 11 additional sight-lines. No value for the column density could be found for the $z_{\text{abs}} = 2.390$ absorber towards B2 0931+31.

² These have been compiled from Davis & May (1978); Brown & Spencer (1979); Briggs & Wolfe (1983); Chengalur & Kanekar (2000); Kanekar et al. (2001a,b, 2009b, 2013, 2014); Briggs et al. (2001); Kanekar & Chengalur (2001, 2003); Curran et al. (2005, 2007, 2010); York et al. (2007); Gupta et al. (2009a,b); Ellison et al. (2012); Srianand et al. (2012); Roy et al. (2013); Kanekar (2014).

3 ANALYSIS

3.1 Spin temperature–covering factor degeneracy

The total neutral atomic hydrogen column density, N_{HI} [cm^{-2}], is related to the velocity integrated optical depth of the H I 21-cm absorption [km s^{-1}] via (Wolfe & Burbridge 1975)

$$N_{\text{HI}} = 1.823 \times 10^{18} T_{\text{spin}} \int \tau dv, \quad (1)$$

where T_{spin} [K] is the harmonic mean spin temperature – the density weighted average of the spin temperature of the absorbing gas along the sight-line. This is a measure of the population of the lower hyperfine level ($F = 1$), where the gas can absorb 21-cm photons (Purcell & Field 1956), relative to the upper hyperfine level ($F = 2$). However, we cannot measure $\int \tau dv$ directly, since the observed optical depth, which is the ratio of the line depth, ΔS , to the observed background flux, S_{obs} , is related to the intrinsic optical depth via

$$\tau \equiv -\ln \left(1 - \frac{\tau_{\text{obs}}}{f} \right) \approx \frac{\tau_{\text{obs}}}{f}, \text{ for } \tau_{\text{obs}} \equiv \frac{\Delta S}{S_{\text{obs}}} \lesssim 0.3, \quad (2)$$

where the covering factor, f , is the fraction of S_{obs} intercepted by the absorber. In the optically thin regime (where $\tau_{\text{obs}} \lesssim 0.3$)³, Equ. 1 can be approximated as

$$N_{\text{HI}} \approx 1.823 \times 10^{18} \frac{T_{\text{spin}}}{f} \int \tau_{\text{obs}} dv. \quad (3)$$

That is, comparison of the 21-cm line strength with the total column density yields the spin temperature degenerate with the covering factor (T_{spin}/f).

In order to obtain the physically interesting spin temperature the covering factor must be known. This requires knowledge of the absorbing cross-section, the extent of the background continuum, as well as the alignment between the absorber and continuum source (see Curran 2017a) and so is generally unknown. Estimates of the covering factor assume that this is equal to the ratio of the compact unresolved component's flux to the total radio flux (e.g. Briggs & Wolfe 1983; Kanekar et al. 2014). However, this gives no information on the depth of the absorption when the extended continuum emission is resolved out nor can it yield information on the absorber and how effectively it covers the emission. This requires high resolution, highly sensitive observations of the absorption across the emission region (e.g. Lane et al. 2000) at low frequencies, thus requiring the Square Kilometre Array (SKA): Phase-1 will be an order of magnitude more sensitive than the GMRT at $z \gtrsim 3$, with phase-2 increasing the sensitivity by another order of magnitude (Curran 2018).

Until such high resolution imaging of the absorption becomes available at the required frequencies, we can use a statistical approach: In the small angle approximation, the covering factor can be obtained from

$$f = \begin{cases} \left(\frac{d_{\text{abs}} DA_{\text{QSO}}}{d_{\text{QSO}} DA_{\text{abs}}} \right)^2 & \text{if } \theta_{\text{abs}} < \theta_{\text{QSO}} \\ 1 & \text{if } \theta_{\text{abs}} \geq \theta_{\text{QSO}}, \end{cases} \quad (4)$$

(Curran 2012), where the angular diameter distance to a source is

$$DA = \frac{DC}{z+1}, \text{ where} \quad (5)$$

³ This applies to all of the DLAs detected in 21-cm absorption, where the observed optical depths span $\tau_{\text{obs}} = 0.05 - 0.26$.

Table 1. The unpublished archival data not completely corrupted by RFI. The name of the background continuum source is followed by its redshift. The redshift and neutral hydrogen column density of the absorber are then given, followed by the observed frequency, GMRT project number, the date of the observation and the total observing time, t_{obs} . ΔS is the rms noise reached per 10 km s⁻¹ channel, S_{obs} is the observed flux density and $\tau_{3\sigma}$ the derived optical depth limit, where $\tau_{3\sigma} = -\ln(1 - 3\Delta S/S_{\text{meas}})$ is quoted for these non-detections.

QSO	z_{QSO}	z_{abs}	$N_{\text{H I}} [\text{cm}^{-2}]$	$\nu_{\text{obs}} [\text{MHz}]$	Proj.	Date	$t_{\text{obs}} [\text{h}]$	$\Delta S [\text{mJy}]$	$S_{\text{obs}} [\text{Jy}]$	$\tau_{3\sigma}$
SDSS J003843.98+031120.8	3.674	3.582	21.60	310.00	24_025	1/9/2013	6.17	20.1	0.338	< 0.178
...	...	3.263	20.29	333.19	24_025	9/8/2013	4.41	17.6	0.345	< 0.153
SDSS J021435.77+015702.8	3.285	2.488	20.88	407.23	30_068	2/9/2016	1.53	21.8	0.125	< 0.741
SDSS J021437.02+063251.3	2.311	2.107	20.80	457.16	30_068	25/8/2016	4.07	8.87	0.058	< 0.614
2MASS J04071807-4410141	3.020	1.9130	20.60	487.61	30_068	2/9/2016	1.97	20.1	0.134	< 0.597
[HB89] 0528-250	2.813	2.1404	21.00	452.30	30_068	5/9/2016	2.00	8.53	0.479	< 0.053
B2 0931+31	2.895	2.390	—	419.00	30_068	1/10/2016	2.31	114	1.050	< 0.390
PKS 1251-407	4.460	3.752	20.30	298.91	24_055	16/9/2013	3.98	33.4	0.454	< 0.221
SDSS J152219.67+211957.3	3.225	3.103	20.55	346.19	24_055	14/5/2013	6.59	129	2.100	< 0.184
SDSS J164208.62+184859.4	3.333	3.150	20.68	342.27	24_055	12/7/2013	3.52	30.7	0.299	< 0.368
...	...	3.223	20.51	336.35	24_055	13/7/2013	6.25	22.5	0.252	< 0.311
WISE J164558.54+633010.8	2.379	2.1253	20.55	454.49	30_068	25/8/2016	1.17	25.7	0.210	< 0.453

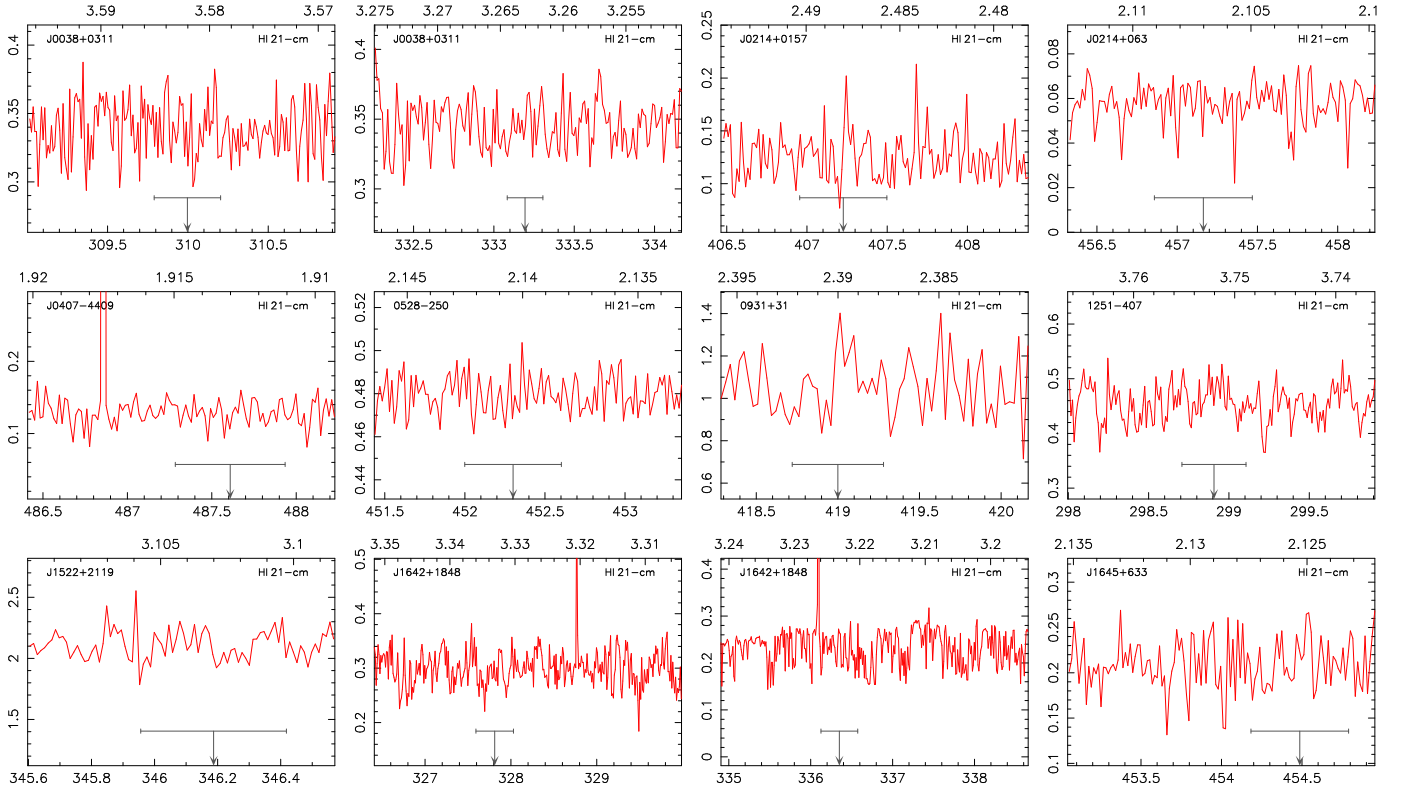


Figure 2. The reduced spectra shown at a spectral resolution of 10 km s⁻¹. The ordinate gives the flux density [Jy] and the abscissa the barycentric frequency [MHz]. The scale along the top shows the redshift of H I 21-cm over the frequency range and the downwards arrow shows the expected frequency of the absorption from the optical redshift, with the horizontal bar showing a span of ± 200 km s⁻¹ for guidance.

$$DC = \frac{c}{H_0} \int_0^z \frac{dz}{\sqrt{\Omega_m(z+1)^3 + (1 - \Omega_m - \Omega_\Lambda)(z+1)^2 + \Omega_\Lambda}}$$

is the line-of-sight co-moving distance (e.g. Peacock 1999), in which c is the speed of light and H_0 the Hubble constant.

For a standard Λ cosmology with $H_0 = 71$ km s⁻¹ Mpc⁻¹, $\Omega_{\text{matter}} = 0.27$ and $\Omega_\Lambda = 0.73$, this gives a peak in the angular diameter distance at $z \approx 1.6$, which has the consequence that below this redshift both $DA_{\text{DLA}} \ll DA_{\text{QSO}}$ and $DA_{\text{DLA}} \sim DA_{\text{QSO}}$ are possible, whereas above $z_{\text{abs}} \sim 1.6$, only $DA_{\text{DLA}} \sim DA_{\text{QSO}}$

is possible. This leads a mix of angular diameter distance ratios ($DA_{\text{abs}}/DA_{\text{QSO}}$) at low redshift but exclusively high ratios ($DA_{\text{abs}}/DA_{\text{QSO}} \sim 1$) at high redshift (Curran & Webb 2006). Thus, there is a clear bias introduced by the geometry of the Universe, which must be accounted for when evaluating the spin temperature. Otherwise this leads to an apparent mix of spin temperatures at $z \lesssim 1$ and exclusively high spin temperatures at $z \gtrsim 1$ (Kaneekar & Chengalur 2003).

For covering factors of less than unity, which is generally expected to be the case (Curran 2017a, see also Kaneekar et al. 2014),

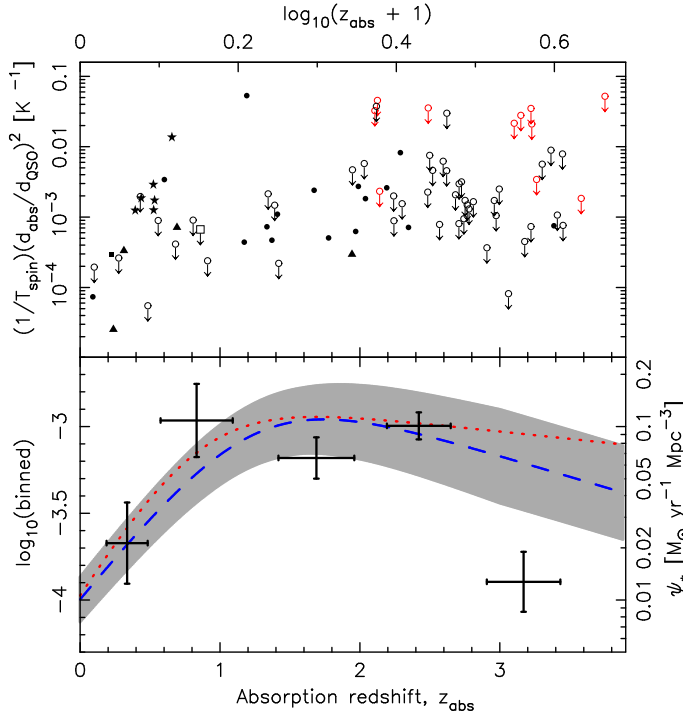


Figure 3. The $(1/T_{\text{spin}})(d_{\text{abs}}/d_{\text{QSO}})^2$ distribution. The top panel shows the individual values, where the filled symbols are those detected in 21-cm absorption and the unfilled 3σ upper limits, with the coloured symbols representing the new data. The shapes indicate the morphology of the absorbing galaxy: star-spiral, square-dwarf, triangle-low surface brightness, circle-unknown. In the bottom panel, the error bars show $\pm 1\sigma$ from the mean (see main text). The right hand scale shows the star formation rate density, with the dotted curve showing the previous fit to the evolution (Fig. 1) and the broken curve a more recent fit, where the shaded region shows the $\pm 1\sigma$ uncertainty (Behroozi et al. 2013).

this gives the spin temperature degenerate with the ratio of the absorber–emitter size,

$$\begin{aligned} \frac{1}{T_{\text{spin}}} \left(\frac{d_{\text{abs}}}{d_{\text{QSO}}} \right)^2 &= \frac{1.823 \times 10^{18}}{N_{\text{HI}}} \left(\frac{DA_{\text{abs}}}{DA_{\text{QSO}}} \right)^2 \int \tau_{\text{obs}} dv \\ &= \frac{1.823 \times 10^{18}}{N_{\text{HI}}} \left(\frac{DA_{\text{abs}}}{DA_{\text{QSO}}} \right)^2 \frac{\Delta S}{S_{\text{obs}}} \Delta v, \end{aligned} \quad (6)$$

where ΔS is the line depth in the case of a detection or $3\sigma_{\text{rms}}$, where σ_{rms} is the r.m.s. noise, per Δv channel for a non-detection.⁴

Adding the new data to the previous gives the distribution shown in Fig. 3. In the binned data, the limits are included via the Kaplan–Meier estimator, a fundamental tenet in non-parametric survival analysis (Kaplan & Meier 1958), which gives a maximum-likelihood estimate based upon the parent population (Feigelson & Nelson 1985). From the binning, we see that the increase in $(T_{\text{spin}})(d_{\text{QSO}}/d_{\text{abs}})^2$ does indeed continue with redshift, although this is somewhat steeper than the decline of the star formation density. However, the decline in ψ_* has also steepened since previous estimates (Hopkins & Beacom 2006 and references therein), due to newer estimates of the dust obscuration of the high

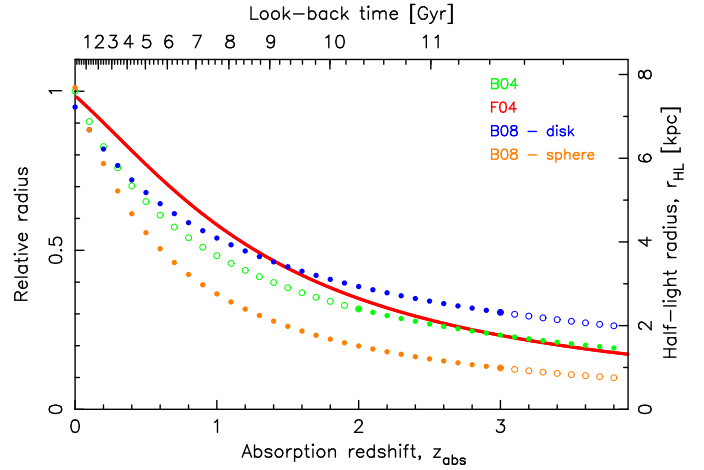


Figure 4. The evolution of massive galaxy size as shown by the fits of F04 (Ferguson et al. 2004), B04 (Bouwens et al. 2004) at $z \geq 2$ and B08 (Buitrago et al. 2008, disk-like and spheroid-like) at $z \leq 3$, where the hollow circles show the extrapolation based upon the observed ranges (full circles). The right hand axis shows the mean half-light radius (Bouwens et al. 2004) to which the other curves are normalised.

redshift ultra-violet photometry (Behroozi et al. 2013). This is confirmed by far-infrared photometry, which is much less attenuated by dust (Burgarella et al. 2013). While the radio-band data are impervious to the effects of intervening dust, the UV emission from the QSO will certainly be attenuated and depletion of metallic species does indicate the presence of dust in DLAs (e.g. Ledoux et al. 2002, but see also Wild et al. 2006), although the degree of reddening suggests that this is low (Murphy & Bernet 2016). Alternatively, in the binning of the data, the high redshift bin contains only a single detection, upon which the censored data are estimated. That is, the high redshift bin may be better considered a lower limit and so further 21-cm detections are required in order to rule out further corrections to the high redshift evolution of ψ_* .

3.2 Absorber size

Aside from this last high redshift bin, the bins in Fig. 3 exhibit some scatter around the star formation rate density fits. This is not unexpected, given that the mean $d_{\text{abs}}/d_{\text{QSO}}$ is assumed to be constant with redshift, which may not be the case: For massive ($\geq 10^{11} M_{\odot}$) galaxies, which are the easiest to resolve at high redshift, there is a well documented evolution in size, where large galaxies dominate the low redshift population (Baker et al. 2000) and dwarf galaxies the high redshift population (Lanfranchi & Friaça 2003), although massive DLA hosts have been observed out to $z \sim 4$ (Djorgovski 1998). Due to hierarchical build-up, one may also expect a size evolution in DLAs and, if similar to the massive galaxies (several low redshift DLAs have been identified as spirals), we expect a similar decrease in size with redshift. Furthermore, both disk and spheroid like galaxies exhibit a decrease in size with redshift (Fig. 4) and, while imaging of DLA hosts is difficult due to the bright background QSO, at low redshift, where this is less challenging, some DLAs have been identified to be spirals (see e.g. Fig. 3).

Since it is close to a mean of the other curves, in addition to providing an absolute size, we use the fit of Bouwens et al. (2004) to evolve the absorber sizes with redshift, i.e. $r_{\text{HL}} = 7.6(z_{\text{abs}} + 1)^{-1.05}$ kpc. This corresponds to $r_{\text{HL}} \approx 8$ kpc at $z \approx 0$ for the

⁴ In the literature the spectral resolutions span a large range of values (Curran 2017b), and so we re-sample the r.m.s. noise levels to a common channel width, which is then used as full-width half maximum (FWHM) of the putative absorption profile.

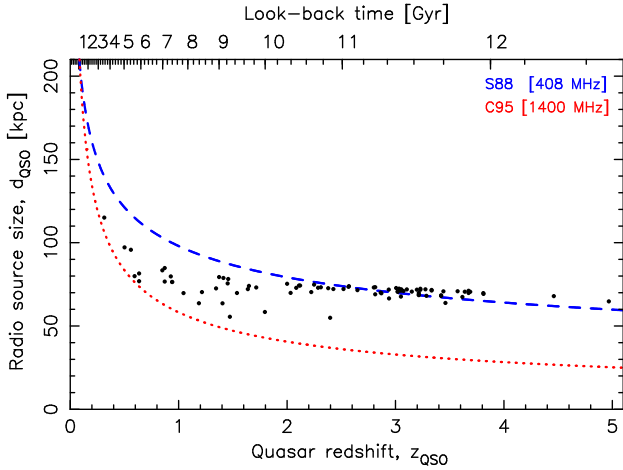


Figure 5. The evolution of quasar size at 408 MHz (S88, Singal 1988) and 1400 MHz (C95, Chyży & Zięba 1995). The circles show the values for the background sources of the sample, obtained by interpolating/extrapolating between the curves.

optical extent of the galaxy, although the H I disk is generally considerably larger than this (Walter et al. 2008). For instance, DLA column densities ($N_{\text{HI}} \gtrsim 10^{20} \text{ cm}^{-2}$) have been mapped to radii of up $r \approx 40 \text{ kpc}$ in nearby galaxies (Bowen et al. 2002; Zwaan et al. 2005a; Curran et al. 2008; Reeves et al. 2015, 2016; Rhodin et al. 2018), including the Milky way (Kalberla & Kerp 2009), as well as in distant ($z \sim 1$) galaxies (Péroux et al. 2011; Bouché et al. 2013). We therefore use an H I radius of $r_{\text{abs}} = 5r_{\text{HL}}$ and evolve this according to Bouwens et al. (2004).

3.3 Radio source size

Quasars also exhibit a redshift evolution, although the size of the source is also dependent upon the observed frequency: The curves in Fig. 5 show the evolution of quasar size at 408 and 1400 MHz.⁵ Converting the power-law fits of the low (Singal 1988) and high (Chyży & Zięba 1995) frequency fits (Fig. 5), we obtain $d_{\text{QSO}} = 97.7 z_{\text{QSO}}^{-0.307}$ at 408 MHz and $d_{\text{QSO}} = 58.2 z_{\text{QSO}}^{-0.520}$ at 1400 MHz, which we interpolate between in order to determine the QSO size at the observed frequency.

4 RESULTS AND DISCUSSION

4.1 Canonical values

Applying the derived $d_{\text{abs}}/d_{\text{QSO}}$ (canonical) ratios to Equ. 4 we obtain the covering factors shown in Fig. 6 and from Equ. 6 the statistical spin temperature,

$$\langle T_{\text{spin}} \rangle = \begin{cases} \frac{N_{\text{HI}}}{1.823 \times 10^{18}} \left(\frac{d_{\text{abs}} DA_{\text{QSO}}}{d_{\text{QSO}} DA_{\text{abs}}} \right)^2 \frac{S_{\text{obs}}}{\Delta S \Delta \nu} & \text{if } \theta_{\text{abs}} < \theta_{\text{QSO}} \\ \frac{N_{\text{HI}}}{1.823 \times 10^{18}} \frac{S_{\text{obs}}}{\Delta S \Delta \nu} & \text{if } \theta_{\text{abs}} \geq \theta_{\text{QSO}}, \end{cases}$$

where $\theta_{\text{abs}} = d_{\text{abs}}/DA_{\text{abs}}$ and $\theta_{\text{QSO}} = d_{\text{QSO}}/DA_{\text{QSO}}$. Applying this to the data gives the distribution shown in Fig. 7, from which we see the binned values of $\langle 1/T_{\text{spin}} \rangle$ tighten around the evolution of ψ_* . This includes the errant high redshift bin, which

⁵ Where we have converted the former (Singal 1988) from the angular sizes using contemporary cosmological parameters (Equ. 5).

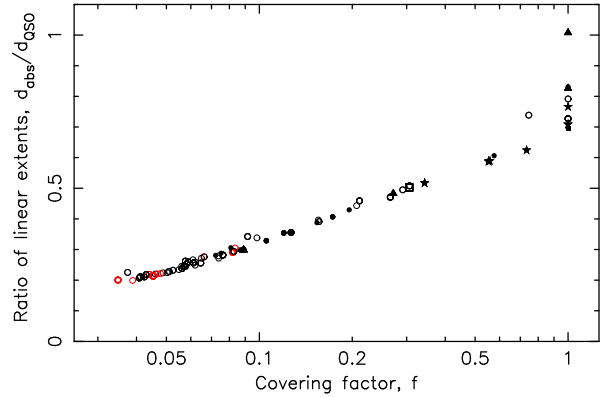


Figure 6. The absorber-quasar size ratio versus the covering factor, for an evolving d_{abs} (Fig. 4) and d_{QSO} (Fig. 5).

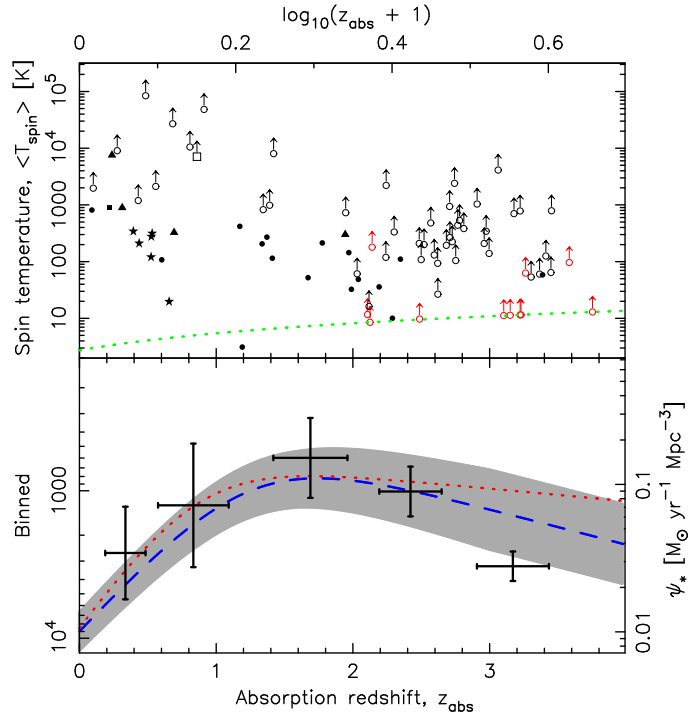


Figure 7. As Fig. 3, but including the statistical values for $d_{\text{abs}}/d_{\text{QSO}}$ and inverted, thus yielding the statistical spin temperature. The dotted line in the top panel shows the lowest possible temperature, due to the CMB at that redshift. The scaling in the bottom panel suggests that $\psi_* \approx 100/T_{\text{spin}} \text{ M}_{\odot} \text{ yr}^{-1} \text{ Mpc}^{-3}$.

now agrees with the star formation density of Behroozi et al. (2013) to within 1σ . Note that there is one point with $T_{\text{spin}} = 3.1 \text{ K}$, which is lower than the temperature of the Cosmic Microwave Background (CMB) expected at $z_{\text{abs}} = 1.191$ ($T_{\text{spin}} = 6.0 \text{ K}$, Muller et al. 2013). This is unphysical, although it should be borne in mind that this is a statistical correction, with the binned values occupying the same range as other studies (Lane & Briggs 2001; Kanekar & Chengalur 2003; Srianand et al. 2012; Roy et al. 2013; Kanekar et al. 2014; Curran et al. 2016), where the covering factor is estimated/assumed.

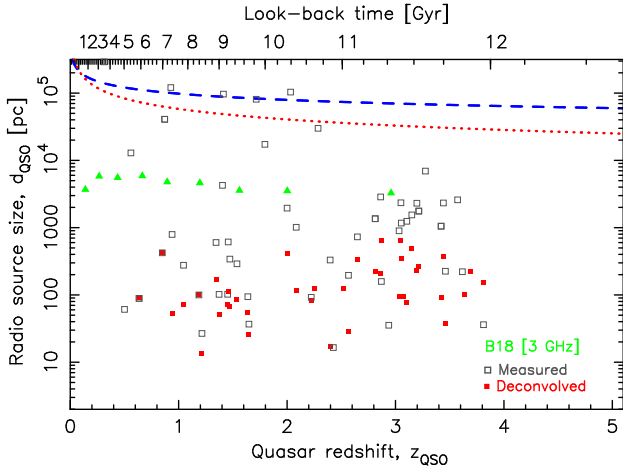


Figure 8. As Fig. 5, but showing the evolution of $> 40 \mu\text{Jy}$ AGN and star-forming galaxies at 3 GHz (Bondi et al. 2018, B08), in addition to the deconvolved (filled squares) and measured (unfilled squares) source sizes for the 21-cm searched DLAs.

4.2 Measured radio extents

While several studies suggest that radio sources evolve from $\sim 100 - 10 \text{ kpc}$ over $z = 0 - 5$ (Nilsson et al. 1993; Singal 1993; Willott et al. 1999; Onah et al. 2018), we now explore the possibility that the source size may be significantly smaller. For example, for radio selected AGN and star-forming galaxies, Bondi et al. (2018) find sizes of $\approx 6 - 3 \text{ kpc}$ over $z = 0 - 3$ for μJy radio selected AGN and star-forming galaxies, although at 3 GHz. Furthermore, 49 of the background sources of the DLAs searched in 21-cm absorption have been imaged at high resolution (Kanekar et al. 2009a, 2013, 2014; Ellison et al. 2012) and found to have sizes of $\approx 0 - 700 \text{ pc}$, which are significantly smaller than those obtained from the source size evolution (Fig. 8). Applying the deconvolved sizes gives the statistical spin temperature distribution shown in Fig. 9, where the covering factor is unity in all cases ($\theta_{\text{abs}} > \theta_{\text{QSO}}$), when using the evolving galaxy model (Fig. 4). While this gives a similar result to the canonical model with $\psi_* \approx 100/T_{\text{spin}} \text{ M}_{\odot} \text{ yr}^{-1} \text{ Mpc}^{-3}$ (Fig. 7) up to the peak of ψ_* , we see a rapid rise in the spin temperature at $z_{\text{abs}} \gtrsim 2$ resulting in a much more severe departure from the evolution of the star formation density.

These sizes are, however, obtained from the deconvolution of the radio images in which the emission is clearly resolved in the convolved synthesised images, leading, in four cases, to unphysical sizes of $\approx 0 \text{ pc}$. Therefore, in Fig. 8 we also show the measured source sizes as obtained directly from the resolved radio images, in conjunction with others from the high resolution Very Large Baseline/Array (VLBI/VLA) observations.⁶ These give the statistical

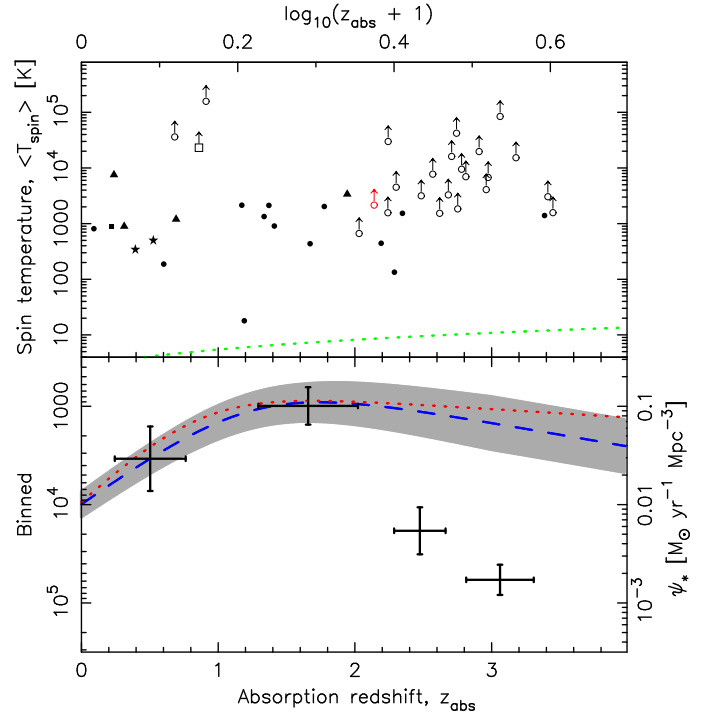


Figure 9. As Fig. 7, but where the deconvolved source sizes are used to obtain d_{QSO} .

spin temperature distribution shown in Fig. 10, which is similar to that of the deconvolved sizes, due to the fact that $f = 1$ for the majority (48 out of 55) of the DLAs.

The difference in the sizes between the general radio source ($\sim 100 \text{ kpc}$) and DLA background ($\sim 10 \text{ kpc}$) populations (Fig. 8) may be due to the high resolution radio images being obtained at high frequencies, where the radio source size will be smaller. This could be particularly acute for the 21-cm absorption, where $\nu_{21\text{-cm}} \ll 1420 \text{ MHz}$ at high redshift. From Fig. 11, we see that this is often the case. Furthermore, high resolution imaging may resolve out all of the extended flux, again underestimating the source size as seen by the absorbing gas.

4.3 Physical implications

For an evolving absorber size, the canonical model and deconvolved/measured radio extents predict very different spin temperatures at high redshift, which may be evident through the degree of ionisation of the neutral gas. For a given number of baryons, an increase in the ionised gas, N_{HII} , will be matched by a decrease in the neutral gas. However, like the general DLA population, there is no evidence of an evolution in the mean column density (Fig. 12), and so we do not expect any significant ionisation over and above that at lower redshift.⁷

The Saha equation (Saha 1921; Fridman 2008) gives the ionisation fraction, the ratio of the number of ions, N_{HII} , to the total

⁶ Compiled from Ulvestad et al. (1981); Perley (1982); Schilizzi et al. (1982); Hintzen et al. (1983); Gower & Hutchings (1984); Stocke et al. (1984); Antonucci & Ulvestad (1985); Rogora et al. (1987); Barthel et al. (1988); Briggs et al. (1989); Neff & Hutchings (1990); Stanghellini et al. (1990); Fejes et al. (1992); van Breugel et al. (1992); Lonsdale et al. (1993); Murphy et al. (1993); Price et al. (1993); Gurvits et al. (1994); Lister et al. (1994); Perlman et al. (1994); Campbell et al. (1995); Polatidis et al. (1995); Reid et al. (1995); Bondi et al. (1996); Chu et al. (1996); Fey et al. (1996); Fey & Charlot (1997); Harvanek et al. (1997); Stanghellini et al. (1997); Shen et al. (1997); Browne et al. (1998); Dallacasa et al. (1998); Saikia et al. (1998); Shen et al. (1998); Tingay et al. (1998); Wilkinson et al. (1998); Reid et al. (1999); Barthel et al. (2000);

Fey & Charlot (2000); Fomalont et al. (2000); Beasley et al. (2002); Helmboldt et al. (2007); Gupta et al. (2012); Srianand et al. (2012).

⁷ Unlike the atomic gas within the host galaxies of high redshift active sources, which is completely ionised at $\gtrsim 10^{56} \text{ ionising photons s}^{-1}$ (Curran & Whiting 2012; Curran et al. 2019).

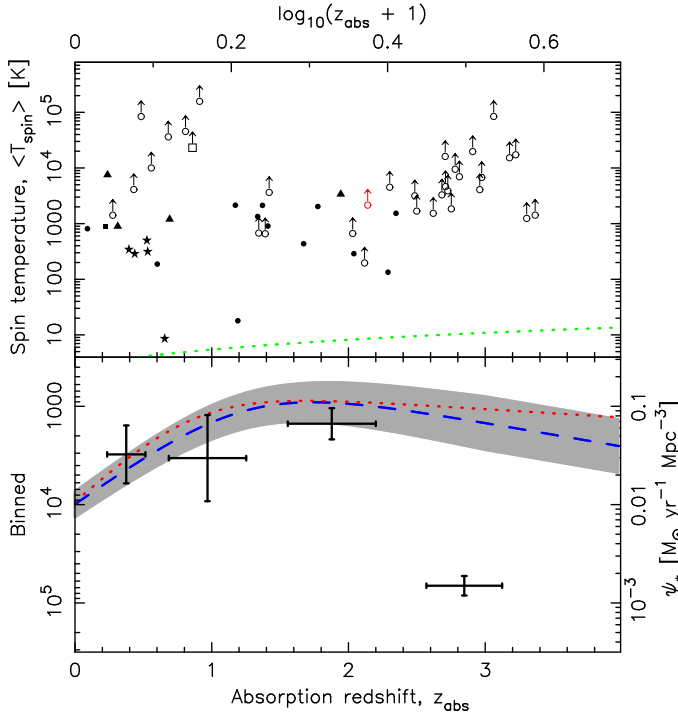


Figure 10. As Fig. 7, but where the measured source sizes are used to obtain d_{QSO} .

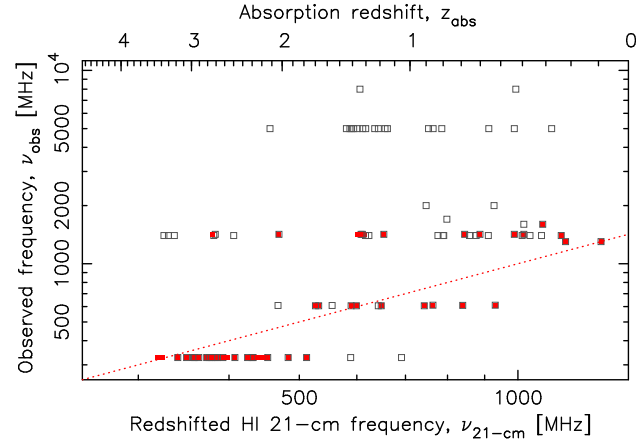


Figure 11. The frequency at which the radio source size is determined versus the redshifted 21-cm frequency. The symbols are as per Fig. 8 and the line shows $\nu_{\text{obs}} = \nu_{21-\text{cm}}$.

number of ions plus atoms, \mathcal{N}_I , at temperature T , as

$$\frac{x^2}{1-x} = \frac{1}{n} \left(\frac{2\pi m_e k T}{h^2} \right)^{3/2} e^{-\phi/kT}, \text{ where } x \equiv \frac{\mathcal{N}_{\text{II}}}{\mathcal{N}_I + \mathcal{N}_{\text{II}}}, \quad (7)$$

with n being the number density of particles [m^{-3}], m_e the mass of the electron, k the Boltzmann constant, h the Planck constant and $\phi = 13.6$ eV the ionisation potential.

Assuming thermodynamic equilibrium across the disk and solving the quadratic in Equ. 7, for an exponential gas disk, $n = n_0 e^{-r/R}$, we obtain the ionisation fraction profiles in Fig. 13. These are shown for the gas distribution of the Milky Way ($n_0 = 13.4 \text{ cm}^{-3}$ and $R_{\text{MW}} = 3.15$ kpc, Kalberla & Kerp 2009), as well as for an evolved absorber size, where we may expect the scale-

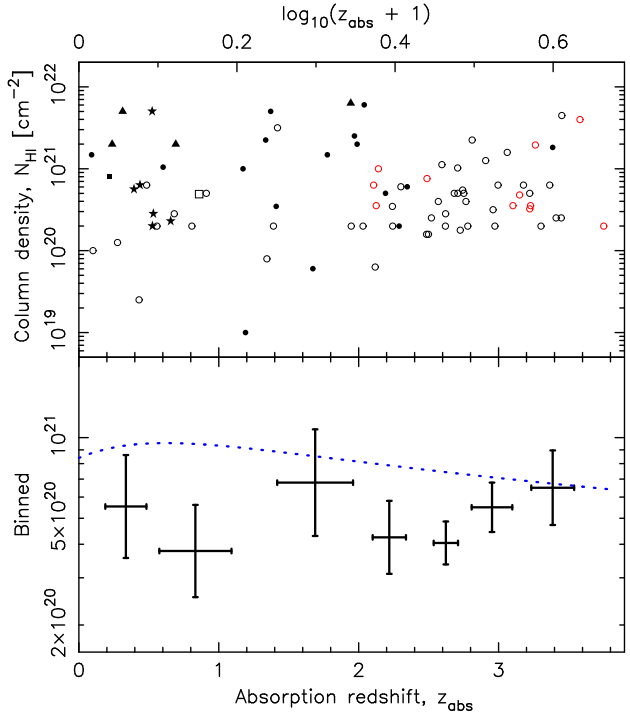


Figure 12. The column density distribution of the DLAs searched in 21-cm absorption. A generalised non-parametric Kendall-tau test gives a probability of $P(\tau) = 0.82$ which is significant at just $S(\tau) = 0.23\sigma$, assuming Gaussian statistics. That is, there is no correlation. In the bottom panel, we show the binned values, with the dotted curve showing the mean column density obtained from the best fit to the cosmological HI mass density of Crighton et al. (2017), $\Omega_{\text{HI}} = 4.0 \times 10^{-4} (z_{\text{abs}} + 1)^{0.60}$ (see Curran 2017b).

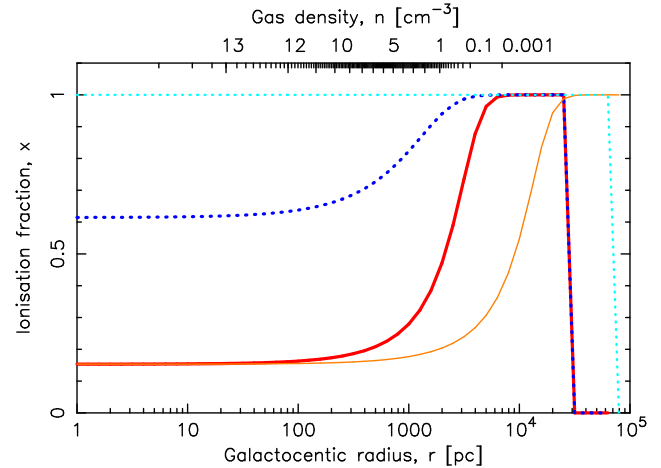


Figure 13. The ionisation fraction versus the galactocentric radius at temperatures of 3250 K and (solid curves) 3500 K (dotted lines) for a central gas density of $n_0 = 13.4 \text{ cm}^{-3}$. The thick traces are for a scale-length of $R = 0.73$ kpc and the thin traces for $R = 3.15$ kpc.

length of the atomic gas density to decrease as $R = R_{\text{MW}}(z_{\text{abs}} + 1)^{-1.05}$, giving $R = 0.73$ kpc at $z \sim 3$ (Sect. 3.2). In either case, the gas completely is ionised at all radii for $T \gtrsim 4000$ K, whereas at $T = 3250$ K (the canonical values, Sect. 4.1) the gas is mostly neutral out to radii of ~ 1 kpc, beyond which the density drops to below $n \sim 1 \text{ cm}^{-3}$.

Although similar to the canonical values at $z_{\text{abs}} \lesssim 2$, the de-

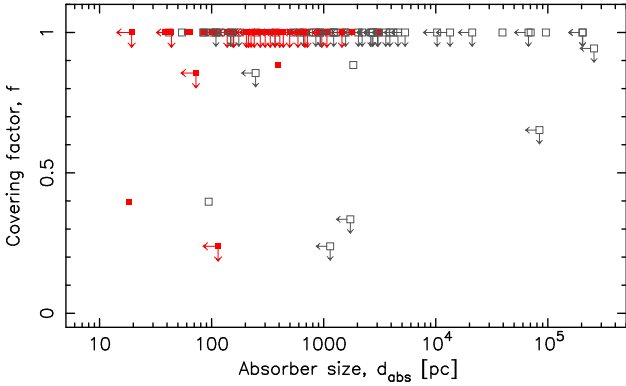


Figure 14. The covering factors and absorber sizes required for a gas temperature of $T = 3000$ K. The symbols are as per Fig. 8, with the limits due to the 21-cm non-detections.

convolved/measured source sizes (Sect. 4.2) in conjunction with the evolved absorber sizes (Sect. 3.2) give much higher statistical spin temperatures at $z_{\text{abs}} \sim 3$ ($T_{\text{spin}} \approx 60\,000$ K). This implies a very high ionisation fraction ($x = 1$), to the point that the strength of the Lyman- α absorption would be below that of Lyman Limit Systems ($N_{\text{HI}} = 10^{17.2} - 10^{20.3} \text{ cm}^{-2}$) at the level of the Lyman- α Forest, contrary to what is observed (Fig. 12).

Dispensing with the evolved absorber sizes, we can use the fact that the gas is mostly neutral to estimate the covering factor required to ensure the gas is below this temperature (Equ. 3), and thus the maximum permitted absorber extent (Equ. 4). From Fig. 14, we see that most of the deconvolved source sizes and many of the measured sizes require absorber extents of $d_{\text{abs}} \lesssim 1$ kpc. This is significantly smaller than those predicted from the evolution of large galaxies, $d_{\text{abs}} \approx 10$ kpc at $z \sim 3$ (Sect. 3.2). Taking the raw values (Fig. 3), the $z \sim 3$ bin gives $T_{\text{spin}}(d_{\text{QSO}}/d_{\text{abs}})^2 \approx 10\,000$ K, which compared with the $T \lesssim 4000$ K limit imposed by the ionisation fraction, gives $d_{\text{QSO}} \gtrsim 2d_{\text{abs}}$.

High redshift imaging of the H I 21-cm emission from DLA hosts is required to verify that the H I disk extends as far past the optical emission at $z \gtrsim 1$ as it does at lower redshift ($d_{\text{abs}} \sim 5d_{\text{HL}}$), although even the SKA will be limited to $z \lesssim 1$ in the detection of 21-cm spectral line emission (Staveley-Smith & Oosterloo 2015). If the case, the above absorption cross-sections imply $d_{\text{HL}} \approx 2$ kpc for the canonical model and $d_{\text{HL}} \lesssim 200$ pc for the measured radio source sizes. DLAs are hypothesised to arise in a multitude of sources, including galactic disks, dwarf galaxies, rapidly rotating proto-disks, merging sub-galactic systems and low surface brightness galaxies (Wolfe et al. 1986; Matteucci et al. 1997; Prochaska & Wolfe 1997; Haehnelt et al. 1998; Jimenez et al. 1999), which does not constrain the above absorption cross-sections. Note, however, that impact parameters of $b \gtrsim 20$ kpc have been found at $z_{\text{abs}} \gtrsim 2$, although identification of DLA hosts is very rare at high redshift (see Fumagalli et al. 2015 and references therein).

5 SUMMARY

We have used unpublished archival GMRT data of H I 21-cm absorption searches in high redshift ($z_{\text{abs}} \gtrsim 2$) damped Lyman- α absorption systems to determine whether the fraction of cold neutral gas continues to trace the star formation density at these redshifts. This adds a dozen new data points, albeit limits, from which

the spin temperature, degenerate with the ratio of the absorber and the continuum source sizes, does increase at high redshift. This is, however, higher than predicted by the star formation density [$T_{\text{spin}}(d_{\text{QSO}}/d_{\text{abs}})^2 \approx 10\,000$ cf. ≈ 2000 K]. This could be explained by an evolution in $d_{\text{QSO}}/d_{\text{abs}}$ and estimating this from the known evolution of galaxy and radio source sizes (the canonical model), gives $\langle T_{\text{spin}} \rangle \approx 3000$ K, cf. $\langle T_{\text{spin}} \rangle \approx 2000$ K expected from the star formation density. This may suggest that the UV data, from which ψ_* is derived at high redshift, is still over-corrected for dust obscuration (Behroozi et al. 2013, cf. Hopkins & Beacom 2006). However, given that there is only a single 21-cm detection in this bin, which forms the parent population with which to incorporate the limits, further $z_{\text{abs}} \gtrsim 3$ detections are required to verify this. Until then, the high redshift bin is best treated as a lower limit to $\langle T_{\text{spin}} \rangle$.

There exists high resolution radio imaging of many of the background QSOs, although applying the galaxy size evolution yields $\langle T_{\text{spin}} \rangle \approx 60\,000$ K at $z_{\text{abs}} \sim 3$, where all of the neutral gas would be ionised, which is inconsistent with the observed flat evolution of the column density. We have used the limiting $T \approx 4000$ K, above which all of the gas is expected to be ionised, to constrain the required absorber extents based upon the high resolution images. These require H I extents of $d_{\text{abs}} \lesssim 1$ kpc, or half-light radii of $r_{\text{HL}} \lesssim 100$ pc, which would support the hypothesis that high redshift DLAs arise predominately in dwarf galaxies, although large impact parameters ($b \gtrsim 20$ kpc) have been found at $z_{\text{abs}} \gtrsim 3$.

The raw values [$T_{\text{spin}}(d_{\text{QSO}}/d_{\text{abs}})^2$], which remove the bias between the low ($z_{\text{abs}} \lesssim 1$) and high redshift samples introduced by the geometry of an expanding Universe, do suggest that the spin temperature, degenerate with the background source-absorber size ratio, traces the star formation density, with the rogue $z_{\text{abs}} \sim 3$ bin being “reigned in” when canonical values of d_{abs} and d_{QSO} are applied. This suggests that $\psi_* T_{\text{spin}} \approx 100 \text{ M}_{\odot} \text{ yr}^{-1} \text{ Mpc}^{-3} \text{ K}$, at least at $z_{\text{abs}} \lesssim 3$. Again, this may be due to the single detection in the parent population or could suggest over-corrections to the UV data, as well as a high redshift variation in the $d_{\text{QSO}}/d_{\text{abs}}$ ratio, perhaps due to a differing ratio in the half-light/H I radii. This could be addressed with further H I 21-cm detections in $z_{\text{abs}} \gtrsim 3$ DLAs, which, although difficult, is feasible with current instruments (Curran 2018).

ACKNOWLEDGEMENTS

I wish to thank the anonymous referee for their helpful comments. This research has made use of the NASA/IPAC Extragalactic Database (NED) which is operated by the Jet Propulsion Laboratory, California Institute of Technology, under contract with the National Aeronautics and Space Administration and NASA’s Astrophysics Data System Bibliographic Service. This research has also made use of NASA’s Astrophysics Data System Bibliographic Service and ASURV Rev 1.2 (Lavalley et al. 1992), which implements the methods presented in Isole et al. (1986).

REFERENCES

- Antonucci R. R. J., Ulvestad J. S., 1985, *ApJ*, 294, 158
- Baker A. C., Mathlin G. P., Churches D. K., Edmunds M. G., 2000, in *Star Formation from the Small to the Large Scale*,

- Vol.45 of ESA SP, Favata F., Kaas A., Wilson A., eds., ESA Special Publication, Noordwijk, p. 21
- Barthel P. D., Miley G. K., Schilizzi R. T., Lonsdale C. J., 1988, *A&AS*, 73, 515
- Barthel P. D., Vestergaard M., Lonsdale C. J., 2000, *A&A*, 354, 7
- Beasley A. J., Gordon D., Peck A. B., Petrov L., MacMillan D. S., Fomalont E. B., Ma C., 2002, *ApJS*, 141, 13
- Behroozi P. S., Wechsler R. H., Conroy C., 2013, *ApJ*, 770, 57
- Bondi M. et al., 1996, *A&A*, 308, 415
- Bondi M. et al., 2018, *A&A*, accepted (arXiv:1810.04095)
- Bouché N., Murphy M. T., Kacprzak G. G., Péroux C., Contini T., Martin C. L., Dessauges-Zavadsky M., 2013, *Science*, 341, 50
- Bouwens R. J., Illingworth G. D., Blakeslee J. P., Broadhurst T. J., Franx M., 2004, *ApJ*, 611, L1
- Bowen D. V., Pettini M., Blades J. C., 2002, *ApJ*, 580, 169
- Braun R., 2012, *ApJ*, 87, 749
- Briggs F. H., de Bruyn A. G., Vermeulen R. C., 2001, *A&A*, 373, 113
- Briggs F. H., Wolfe A. M., 1983, *ApJ*, 268, 76
- Briggs F. H., Wolfe A. M., Liszt H. S., Davis M. M., Turner K. L., 1989, *ApJ*, 341, 650
- Brown R. L., Spencer R. E., 1979, *ApJ*, 230, L1
- Browne I. W. A., Wilkinson P. N., Patnaik A. R., Wrobel J. M., 1998, *MNRAS*, 293, 257
- Buitrago F., Trujillo I., Conselice C. J., Bouwens R. J., Dickinson M., Yan H., 2008, *ApJ*, 687, L61
- Burgarella D. et al., 2013, *A&A*, 554, A70
- Campbell R. M., Lehar J., Corey B. E., Shapiro I. I., Falco E. E., 1995, *AJ*, 110, 2566
- Chengalur J. N., Kanekar N., 2000, *MNRAS*, 318, 303
- Chu L. B., Bååth F. T., Rantakyrö F. J., Zhang H. S., Nicholson G., 1996, *A&A*, 307, 15
- Chyży K. T., Zięba S., 1995, *A&A*, 303, 420
- Crighton N. H. M. et al., 2017, in *IAU Symposium*, Vol. 321, *Formation and Evolution of Galaxy Outskirts*, Gil de Paz A., Knapen J. H., Lee J. C., eds., pp. 309–314
- Curran S. J., 2012, *ApJ*, 748, L18
- Curran S. J., 2017a, *MNRAS*, 470, 3159
- Curran S. J., 2017b, *A&A*, 606, A56
- Curran S. J., 2018, *PASA*, 35, 36
- Curran S. J., Hunstead R. W., Johnston H. M., Whiting M. T., Sadler E. M., Allison J. R., Athreya R., 2019, *MNRAS*, 484, 1182
- Curran S. J., Koribalski B. S., Bains I., 2008, *MNRAS*, 389, 63
- Curran S. J., Murphy M. T., Pihlström Y. M., Webb J. K., Purcell C. R., 2005, *MNRAS*, 356, 1509
- Curran S. J., Reeves S. N., Allison J. R., Sadler E. M., 2016, *MNRAS*, 459, 4136
- Curran S. J., Tzanavaris P., Darling J. K., Whiting M. T., Webb J. K., Bignell C., Athreya R., Murphy M. T., 2010, *MNRAS*, 402, 35
- Curran S. J., Tzanavaris P., Pihlström Y. M., Webb J. K., 2007, *MNRAS*, 382, 1331
- Curran S. J., Webb J. K., 2006, *MNRAS*, 371, 356
- Curran S. J., Whiting M. T., 2012, *ApJ*, 759, 117
- Dallacasa D., Bondi M., Alef W., Mantovani F., 1998, *A&AS*, 129, 219
- Davis M. M., May L. S., 1978, *ApJ*, 219, 1
- Delhaize J., Meyer M. J., Staveley-Smith L., Boyle B. J., 2013, *MNRAS*, 433, 1398
- Djorgovski S. G., 1998, in *Structure et Evolution du Milieu Inter-Galactique Revele par Raies D’Absorption dans le Spectre des Quasars*, 13th Colloque d’Astrophysique de l’Institut d’Astrophysique de Paris, p. 303
- Ellison S., Kanekar N., and Prochaska J. X., Momjian E., Worseck G., 2012, *MNRAS*, 424, 293
- Feigelson E. D., Nelson P. I., 1985, *ApJ*, 293, 192
- Fejes I., Porcas R. W., Akujor C. E., 1992, *A&A*, 257, 459
- Ferguson H. C. et al., 2004, *ApJ*, 600, L107
- Fey A. L., Charlot P., 1997, *ApJS*, 111, 95
- Fey A. L., Charlot P., 2000, *ApJS*, 128, 17
- Fey A. L., Clegg A. W., Fomalont E. B., 1996, *ApJS*, 105, 299
- Fomalont E. B., Frey S., Paragi Z., Gurvits L. I., Scott W. K., Taylor A. R., Edwards P. G., Hirabayashi H., 2000, *ApJS*, 131, 95
- Fridman A. A., 2008, *Plasma Chemistry*. Cambridge University Press
- Fumagalli M., O’Meara J. M., Prochaska J. X., Rafelski M., Kanekar N., 2015, *MNRAS*, 446, 3178
- Gower A. C., Hutchings J. B., 1984, *AJ*, 89, 1658
- Gupta N., Srianand R., Petitjean P., Bergeron J., Noterdaeme P., Muzahid S., 2012, *A&A*, 544, 21
- Gupta N., Srianand R., Petitjean P., Noterdaeme P., Saikia D. J., 2009a, in *Astronomical Society of the Pacific Conference Series*, Vol. 407, *The Low-Frequency Radio Universe*, Saikia D. J., Green D. A., Gupta Y., Venturi T., eds., p. 67
- Gupta N., Srianand R., Petitjean P., Noterdaeme P., Saikia D. J., 2009b, *MNRAS*, 398, 201
- Gurvits L. I., Schilizzi R. T., Barthel P. D., Kardashev N. S., Kellermann K. I., Lobanov A. P., Pauliny-Toth I. I. K., Popov M. V., 1994, *A&A*, 291, 737
- Haehnelt M. G., Steinmetz M., Rauch M., 1998, *ApJ*, 495, 647
- Harvanek M., Stocke J. T., Morse J. A., Rhee G., 1997, *AJ*, 114, 2240
- Helmboldt J. F. et al., 2007, *ApJ*, 658, 203
- Hintzen P., Ulvestad J., Owen F., 1983, *AJ*, 88, 709
- Hopkins A. M., Beacom J. F., 2006, *ApJ*, 651, 142
- Hoppmann L., Staveley-Smith L., Freudling W., Zwaan M. A., Minchin R. F., Calabretta M. R., 2015, *MNRAS*, 452, 3726
- Isobe T., Feigelson E., Nelson P., 1986, *ApJ*, 306, 490
- Jimenez R., Bowen D. V., Matteucci F., 1999, *ApJ*, 514, L83
- Kalberla P. M. W., Kerp J., 2009, *Ann. Rev. Astr. Ap.*, 47, 27
- Kanekar N., 2014, *ApJ*, 797, L20
- Kanekar N., Chengalur J. N., 2001, *A&A*, 369, 42
- Kanekar N., Chengalur J. N., 2003, *A&A*, 399, 857
- Kanekar N., Chengalur J. N., Subrahmanyan R., Petitjean P., 2001a, *A&A*, 367, 46
- Kanekar N., Ellison S. L., Momjian E., York B. A., Pettini M., 2013, *MNRAS*, 532
- Kanekar N., Ghosh T., Chengalur J. N., 2001b, *A&A*, 373, 394
- Kanekar N., Lane W. M., Momjian E., Briggs F. H., Chengalur J. N., 2009a, *MNRAS*, 394, L61
- Kanekar N., Prochaska J. X., Ellison S. L., Chengalur J. N., 2009b, *MNRAS*, 396, 385
- Kanekar N. et al., 2014, *MNRAS*, 438, 2131
- Kaplan E. L., Meier P., 1958, *J. Amer. Statist. Assoc.*, 53, 457
- Lah P. et al., 2007, *MNRAS*, 376, 1357
- Lane W. M., Briggs F. H., 2001, *ApJ*, 561, L27
- Lane W. M., Briggs F. H., Smette A., 2000, *ApJ*, 532, 146
- Lanfranchi G. A., Friaça A. C. S., 2003, *MNRAS*, 343, 481
- Lavalley M. P., Isobe T., Feigelson E. D., 1992, in *BAAS*, Vol. 24, pp. 839–840
- Ledoux C., Bergeron J., Petitjean P., 2002, *A&A*, 385, 802
- Lister M. L., Gower A. C., Hutchings J. B., 1994, *AJ*, 108, 821

- Lonsdale C. J., Barthel P. D., Miley G. K., 1993, *ApJS*, 87, 63
- Madau P., Dickinson M., 2014, *Ann. Rev. Astr. Ap.*, 52, 415
- Matteucci F., Molaro P., Vladilo G., 1997, *A&A*, 321, 45
- Muller S. et al., 2013, *A&A*, 109
- Murphy D. W., Browne I. W. A., Perley R. A., 1993, *MNRAS*, 264, 298
- Murphy M. T., Bernet M. L., 2016, *MNRAS*, 455, 1043
- Neff S. G., Hutchings J. B., 1990, *AJ*, 100, 1441
- Nilsson K., Valtonen M. J., Kotilainen J., Jaakkola T., 1993, *ApJ*, 413, 453
- Onah C. I., Ubachukwu A. A., Odo F. C., Onuchukwu C. C., 2018, *Revista Mexicana de Astronomía y Astrofísica*, 54, 271
- Peacock J. A., 1999, *Cosmological Physics*. Cambridge University Press, Cambridge
- Perley R. A., 1982, *AJ*, 87, 859
- Perlman E. S., Stocke J. T., Shaffer D. B., Carilli C. L., Ma C., 1994, *ApJ*, 424, L69
- Péroux C., Bouché N., Kulkarni V. P., York D. G., Vladilo G., 2011, *MNRAS*, 410, 2251
- Polatidis A. G., Wilkinson P. N., Xu W., Readhead A. C. S., Pearson T. J., Taylor G. B., Vermeulen R. C., 1995, *ApJS*, 98, 1
- Price R., Gower A. C., Hutchings J. B., Talon S., Duncan D., Ross G., 1993, *ApJS*, 86, 365
- Prochaska J. X., Herbert-Fort S., Wolfe A. M., 2005, *ApJ*, 635, 123
- Prochaska J. X., Wolfe A. M., 1997, *ApJ*, 487, 73
- Purcell E. M., Field G. B., 1956, *ApJ*, 124, 542
- Rao S. M., Turnshek D. A., Sardane G. M., Monier E. M., 2017, *MNRAS*, 471, 3428
- Reeves S. N., Sadler E. M., Allison J. R., Koribalski B. S., Curran S. J., Pracy M. B., 2015, *MNRAS*, 450, 926
- Reeves S. N., Sadler E. M., Allison J. R., Koribalski B. S., Curran S. J., Pracy M. B., 2016, *MNRAS*, 457, 2613
- Reid A., Shone D. L., Akujor C. E., Browne I. W. A., Murphy D. W., Pedelty J., Rudnick L., Walsh D., 1995, *A&AS*, 110, 213
- Reid R. I., Kronberg P. P., Perley R. A., 1999, *ApJS*, 124, 285
- Rhee J., Zwaan M. A., Briggs F. H., Chengalur J. N., Lah P., Oosterloo T., van der Hulst T., 2013, *MNRAS*, 435, 2693
- Rhodin N. H. P., Christensen L., Møller P., Zafar T., Fynbo J. P. U., 2018, *A&A*, accepted (arXiv:1807.01755)
- Rogora A., Padrielli L., de Ruiter H. R., 1987, *A&AS*, 67, 267
- Roy N., Mathur S., Gajjar V., Nath Patra N., 2013, *MNRAS*, 436, L94
- Saha M. N., 1921, *Proceedings of the Royal Society of London Series A*, 99, 135
- Saikia D. J., Holmes G. F., Kulkarni A. R., Salter C. J., Garrington S. T., 1998, *MNRAS*, 298, 877
- Schilizzi R. T., Kapahi V. K., Neff S. G., 1982, *JA&A*, 3, 173
- Shen Z.-Q., Wan T.-S., Moran J. M., Jauncey D. L., Reynolds J. E., Tzioumis A. K., 1997, *AJ*, 114, 1999
- Shen Z.-Q., Wan T.-S., Moran J. M., Jauncey D. L., Reynolds J. E., Tzioumis A. K., 1998, *AJ*, 115, 1357
- Singal A. K., 1988, *MNRAS*, 233, 87
- Singal A. K., 1993, *MNRAS*, 263, 139
- Sobral D., Smail I., Best P. N., Geach J. E., Matsuda Y., Stott J. P., Cirasuolo M., Kurk J., 2013, *MNRAS*, 428, 1128
- Srianand R., Gupta N., Petitjean P., Noterdaeme P., Ledoux C., Salter C. J., Saikia D. J., 2012, *MNRAS*, 421, 651
- Stanghellini C., Baum S. A., O’Dea C. P., Morris G. B., 1990, *A&A*, 233, 379
- Stanghellini C., O’Dea C. P., Baum S. A., Dallacasa D., Fanti R., Fanti C., 1997, *A&A*, 325, 943
- Staveley-Smith L., Oosterloo T., 2015, *Advancing Astrophysics with the Square Kilometre Array (AASKA14)*, 167
- Stocke J. T., Foltz C. B., Weymann R. J., Christiansen W. A., 1984, *ApJ*, 280, 476
- Tingay S. J. et al., 1998, *ApJ*, 497, 594
- Ulvestad J., Johnston K., Perley R., Fomalont E., 1981, *AJ*, 86, 1010
- van Breugel W. J. M., Fanti C., Fanti R., Stanghellini C., Schilizzi R. T., Spencer R. E., 1992, *A&A*, 256, 56
- Walter F., Brinks E., de Blok W. J. G., Bigiel F., Kennicutt, Jr. R. C., Thornley M. D., Leroy A., 2008, *AJ*, 136, 2563
- Wild V., Hewett P. C., Pettini M., 2006, *MNRAS*, 367, 211
- Wilkinson P. N., Browne I. W. A., Patnaik A. R., Wrobel J. M., Sorathia B., 1998, *MNRAS*, 300, 790
- Willott C. J., Rawlings S., Blundell K. M., Lacy M., 1999, *MNRAS*, 309, 1017
- Wolfe A. M., Burbidge G. R., 1975, *ApJ*, 200, 548
- Wolfe A. M., Turnshek D. A., Smith H. E., Cohen R. D., 1986, *ApJS*, 61, 249
- York B. A., Kanekar N., Ellison S. L., Pettini M., 2007, *MNRAS*, 382, L53
- Zwaan M. A., Meyer M. J., Staveley-Smith L., Webster R. L., 2005a, *MNRAS*, 359, L30
- Zwaan M. A., van der Hulst J. M., Briggs F. H., Verheijen M. A. W., Ryan-Weber E. V., 2005b, *MNRAS*, 364, 1467
- Zwart J. T. L., Jarvis M. J., Deane R. P., Bonfield D. G., Knowles K., Madhanpall N., Rahmani H., Smith D. J. B., 2014, *MNRAS*, 439, 1459